



Predicting the LISA white dwarf binary population in the Milky Way with cosmological simulations

Astrid Lamberts^{1,2*} Sarah Blunt,^{3,4†} Tyson B. Littenberg,⁵
Shea Garrison-Kimmel^{1,2} Thomas Kupfer⁶ and Robyn E. Sanderson^{1,7,8}

¹Université Côte d'Azur; Observatoire de la Côte d'Azur; CNRS, Laboratoire Lagrange, Laboratoire Artémis 06304, France

²Theoretical Astrophysics (TAPIR), California Institute of Technology, Pasadena, CA 91125, USA

³California Institute of Technology, Pasadena, CA 91125, USA

⁴Center for Astrophysics | Harvard & Smithsonian, Cambridge, MA 02138, USA

⁵NASA Marshall Space Flight Center, Huntsville, AL 35812, USA

⁶Kavli Institute for Theoretical Physics, University of California, Santa Barbara, CA 93106, USA

⁷Department of Physics & Astronomy, University of Pennsylvania, 209 S 33rd St., Philadelphia, PA 19104, USA

⁸Center for Computational Astrophysics, Flatiron Institute, 162 5th Ave, New York, NY 10010, USA

Accepted 2019 October 2. Received 2019 September 12; in original form 2019 June 28

ABSTRACT

White dwarf binaries with orbital periods below 1 h will be the most numerous sources for the space-based gravitational wave detector *Laser Interferometer Space Antenna* (*LISA*). Based on thousands of individually resolved systems, we will be able to constrain binary evolution and provide a new map of the Milky Way and its close surroundings. In this paper we predict the main properties of populations of different types of detached white dwarf binaries detected by *LISA* over time. For the first time, we combine a high-resolution cosmological simulation of a Milky Way-mass galaxy (taken from the FIRE project) with a binary population synthesis model for low- and intermediate-mass stars. Our Galaxy model therefore provides a cosmologically realistic star formation and metallicity history for the Galaxy and naturally produces its different components such as the thin and thick disc, the bulge, the stellar halo, and satellite galaxies and streams. Thanks to the simulation, we show how different Galactic components contribute differently to the gravitational wave signal, mostly due to their typical age and distance distributions. We find that the dominant *LISA* sources will be He–He double white dwarfs (DWDs) and He–CO DWDs with important contributions from the thick disc and bulge. The resulting sky map of the sources is different from previous models, with important consequences for the searches for electromagnetic counterparts and data analysis. We also emphasize that much of the science-enabling information regarding white dwarf binaries, such as the chirp mass and the sky localization, becomes increasingly rich with long observations, including an extended mission up to 8 yr.

Key words: gravitational waves – binaries: close – white dwarfs – Galaxy: stellar content.

1 INTRODUCTION

Gravitational waves (GW) are the most promising way towards systematic detection of compact binaries. The LIGO/Virgo detectors have observed the mergers of several binary black holes (The LIGO Scientific Collaboration 2018) and a binary neutron star (Abbott et al. 2017), emitting GW in the kiloHertz regime. Within the next 20 yr the *Laser Interferometer Space Antenna* (*LISA*) will open up

a new window in the GW spectrum, between 10^{-5} and 10^{-2} Hz (Amaro-Seoane et al. 2017). By numbers, the dominant sources for *LISA* will be double white dwarfs (DWDs) in our Milky Way (MW), about a hundred thousand years before they merge. As white dwarfs (WDs) are the remnants of stars below $\lesssim 8 M_{\odot}$, more than 95 per cent of the stars are likely to end their lives as WDs.

In a seminal paper, Nelemans, Yungelson & Portegies Zwart (2001b) determined several tens of millions of detached DWDs would be present in the *LISA* band and roughly ten thousand of them, with GW frequency $f_{\text{GW}} \gtrsim 0.4$ mHz, would be individually resolvable. With (at least) thousands of detectable systems, *LISA* will allow new statistical studies of close DWDs. Such studies will

* E-mail: astrid.lamberts@oca.eu

† NSF Graduate Research Fellow.

strongly advance our understanding of stellar and binary evolution. The distribution of chirp masses and periods will allow to constrain the impact of the common envelope, which drastically tightens the orbit of the systems (Toonen et al. 2014b). A complete sample will also allow for a direct comparison with the post-common envelope binaries, which have undergone only one episode of the common envelope (Rebassa-Mansergas et al. 2012). In some cases, the frequency derivative will be measurable and will allow to determine if mass transfer is happening (Marsh, Nelemans & Steeghs 2004; Gokhale, Peng & Frank 2007; Kremer et al. 2017) and/or tidal interactions are deforming the white dwarfs.

GW observations are very complementary to electromagnetic (EM) observations, which are challenging as WDs are faint and rapidly cool down to become even fainter. Even with dedicated surveys, our view of DWDs in the MW is going to be hindered by dust extinction and faintness of the sources before the start of *LISA* operations. Short period binaries observable by *LISA* (orbital period below half an hour) are found with phase-resolved spectroscopy of previously discovered white dwarfs (Napiwotzki et al. 2001; Brown et al. 2010a, 2016b) or light curves from high-cadence surveys (Levitin et al. 2013). Roughly 20 DWDs have been discovered with a high enough frequency to be detectable by *LISA*. Most of these binaries are interacting binaries, which are a rare sub-class but are easier to detect electromagnetically because of the presence of an accretion disc (Nelemans et al. 2001b). These electromagnetically identified binaries are called ‘verification binaries’ and are guaranteed multimessenger sources (see Kupfer et al. 2018, for an updated list using *Gaia* distances). Large-scale systematic searches for these high-frequency systems are just starting, with e.g. the high-cadence survey ZTF (Zwicky Transient Factory; Bellm et al. 2019; Graham et al. 2019) and possibly LSST (Large Synoptic Survey Telescope) although a survey of the Galactic plane has not been optimized yet (Strader et al. 2018; Street et al. 2018).

DWDs will be a new way to look at our MW, showing a population of older, low-mass stars. As the strain amplitude of GW decreases only as $1/r$ (in comparison to $1/r^2$ decrease for EM emission), *LISA* will be able to more easily sample more remote regions of our Galaxy, its satellite and maybe Andromeda (Cooray & Seto 2005; Korol, Koop & Rossi 2018). The *LISA* detections could lead to a new measurement of the Galactic potential (Korol, Rossi & Barausse 2019) and the global amplitude of the signal due to DWDs will quantify the star formation history of the MW (Yu & Jeffery 2013).

Aside from their importance for stellar/binary evolution and the Galactic structure, predicting and understanding the GW detections of DWDs is crucial to the success of the *LISA* mission. Most of the DWDs will be unresolved, meaning there will be more than one binary emitting in a given frequency bin, which width is set by the inverse of the observation time (roughly the duration of the mission). Below $\simeq 2$ mHz, the combination of these unresolved sources will effectively be a contaminating foreground which will prevent or hinder the detection of other sources such as extreme mass ratio inspirals or supermassive black hole mergers at low masses (Nelemans et al. 2001b; Ruiter et al. 2010; Marsh 2011; Nissanke et al. 2012).

Since the first predictions based on a Galaxy model combined with a binary population model (Nelemans et al. 2001b,a), models have included detailed studies of different DWD formation channels (Nissanke et al. 2012), the different types of DWDs and their spatial distribution in the MW (Ruiter et al. 2010). Important uncertainties remain regarding binary evolution (Postnov & Yungelson 2014), although the volume of observational completeness in our

neighbourhood is slowly increasing and is a promising way to put constraints (Toonen et al. 2017). More recent studies demonstrate the potential of multimessenger detections and the link with *Gaia* and LSST (Korol et al. 2017; Breivik et al. 2018). Korol et al. (2019) predicts that *Gaia* will detect about 25 verification binaries within 2 kpc, and LSST about 50 more, within 10 kpc; and that most of them will be away from the Galactic plane and bulge.

All these studies are based on parametrized models for the MW’s star formation and structure. They use axisymmetric models for the different components of the Galaxy, which often only model the thin disc and bulge. The star formation rate follows a simple parametrization: a constant in Ruiter et al. (2010), an exponential decrease in Yu & Jeffery (2010) or the Prantzos & Boissier (2000) star formation model of the MW in Nelemans et al. (2001a), Nissanke et al. (2012), and Korol et al. (2017). Calculations are performed assuming a unique value of the metallicity for each Galactic component. Ruiter et al. (2009) first highlighted that different Galactic components have different contributions to the GW signal because of their different age, metallicity, and typical distances. These findings motivate the present analysis, where we combine a binary population synthesis model with a cosmological hydrodynamic simulation of an MW-like galaxy (Wetzel et al. 2016) to model the structure and star formation history. This allows us to naturally include all the components of the MW such as the thin and thick disc, the bulge and the accreted stellar halo, as well as a population of satellite galaxies. A similar approach for binary black holes (Lamberts et al. 2018) has shown that the latter are over-represented in the stellar halo of the Galaxy, where the metallicity is low.

This paper builds on the methodology developed in Lamberts et al. (2018) combining synthetic binary black hole populations with the same cosmological simulations (Section 2). We will show the resulting detached DWD populations and how their main properties stem from binary evolution and galactic structure and evolution (Section 3). We will highlight the impact of a complete Galactic model for the detection of GW with *LISA* (Section 4) and compare it with previous results (Section 5) and conclude (Section 6).

2 METHOD

We follow the same method as Lamberts et al. (2018), built on a set of simulations of MW-like galaxies (Section 2.1) and a binary population synthesis model (Section 2.2) uniquely combined together (Section 2.3) to make GW predictions (Section 2.4).

2.1 FIRE Galaxy model

We use a subset of MW-like galaxies from the Feedback in Realistic Environment (FIRE; Hopkins et al. 2014) project,¹ including **m12i** (*a.k.a.* the ‘Latte’ simulation; Wetzel et al. 2016, **m12m** and **m12f** (Garrison-Kimmel et al. 2017) simulations. These simulations are based on the improved ‘FIRE-2’ version of the code from Hopkins et al. (2018, for details, see Section 2 therein) and ran with the code GIZMO (Hopkins 2015).² GIZMO solves the equations of hydrodynamics using the mesh-free Lagrangian Godunov ‘MFM’ method. The analysis of the simulations is done with the publicly available Python package GIZMO_ANALYSIS.

¹<http://fire.northwestern.edu>

²<http://www.tapir.caltech.edu/~phopkins/Site/GIZMO.html>

More specifically, these simulations have an initial gas particle mass of about $7070 M_{\odot}$ and for the gas, both the hydrodynamic and gravitational (force softening) resolutions are fully adaptive down to 1 pc. The simulations include cooling and heating from a meta-galactic background and local stellar sources from $T \sim 10\text{--}10^{10}$ K. Star formation occurs in locally self-gravitating, dense, self-shielding molecular, Jeans-unstable gas. Stellar feedback from OB and AGB star mass-loss, type Ia and II supernovae, and multiwavelength photoheating and radiation pressure is directly based on stellar evolution models. Chemical enrichment stems from type Ia supernovae (Iwamoto et al. 1999), core-collapse supernovae (Nomoto et al. 2006), and O and AGB star winds (van den Hoek & Groenewegen 1997; Marigo 2001; Izzard et al. 2004). The simulations include subgrid-scale numerical turbulent metal diffusion terms (Bonaca et al. 2017; Hopkins et al. 2018), which have almost no dynamical effect at the galaxy mass scales considered here (Su et al. 2017), but produce better agreement with the internal metallicity distribution functions observed in MW satellite galaxies (Escala et al. 2018). All the binary evolution models are included during post-processing, and the hydrodynamic simulation does not explicitly include binary effects.

Our analysis is based on galaxy **m12i** (from Wetzel et al. 2016), though we analyse a re-simulation with turbulent metal diffusion first presented in Bonaca et al. 2017, chosen to have a merger history comparable to the Milky Way. We also consider a lower resolution version of **m12i** as well as two different galaxies **m12f** and **m12m** (Hopkins et al. 2018) at the same mass scale. **m12i** shows metallicity gradients (Ma et al. 2017) and abundances of α -elements (Wetzel et al., in prep.) in the disc that are broadly consistent with observations of the MW. Its global star formation history is consistent with the MW (see Ma et al. 2017 for illustrations) although its present-day star formation rate of $6 M_{\odot} \text{ yr}^{-1}$ is somewhat higher than observed in the Milky Way. The satellite distribution around the main galaxy in **m12i** presents a similar mass and velocity distribution as observed around the Milky Way and M31, down to a stellar mass of $10^5 M_{\odot}$, though the simulation does not contain an equivalent of the Large Magellanic Cloud; the most massive satellite is comparable to the Small Magellanic Cloud. Outputs from the simulations and corresponding mock *Gaia* catalogues are available online,³ based on Sanderson et al. (2018), which also compares the simulated galaxies with the Milky Way. Effectively our analysis is based on this publicly available data, except for the information on the location of the stars at their formation, which have been obtained with permission.

From the simulation, we recover the position, formation time t_* , metallicity Z and position and mass at formation M_* of every star particle.⁴ We only use the particles within 300 kpc of the centre of the galaxy. This is slightly larger than the virial radius of the galaxy and allows us to largely sample the halo, satellites, and streams while remaining unaffected by the boundaries of the high-resolution region. This yields a list of roughly 14 million star particles.

The simulations assume a Λ cold dark matter cosmology with $\Omega_{\Lambda} = 0.728$, $\Omega_m = 0.272$, $\Omega_b = 0.0455$, $h = 0.702$, $\sigma_8 = 0.807$, and $n_s = 0.961$ (Planck Collaboration XIII 2016). All metallicities are defined with respect to the solar metallicity, set to $Z_{\odot} = 0.02$.

³<https://fire.northwestern.edu/data/> and <http://ananke.hub.yt>

⁴Whenever we refer to the simulation, we use the words star, particle and star particle interchangeably.

2.2 Binary population synthesis model (BPS)

To simulate a population of DWDs, we use a modified version of the publicly available BINARY STAR EVOLUTION (BSE) code based on the rapid binary evolution algorithm described in Hurley, Tout & Pols (2002b). We only consider formation through binary evolution as the survival of compact low-mass binaries is unlikely in dense stellar environments. For low-mass binaries (see Postnov & Yungelson 2014, for a recent review), the main uncertainty stems from our limited understanding of the common envelope phase (Ivanova et al. 2013).

As in Lamberts et al. (2018) we model 13 logarithmically spaced metallicity bins between 5×10^{-3} and $1.6 Z_{\odot}$. We model a distribution with a thermal eccentricity (Heggie 1975), which favours systems with high eccentricity and model a distribution of initial separations between 1 and $10^6 R_{\odot}$ following a flat distribution in log space (Abt 1983). Primary masses m_{1*} are drawn from a Kroupa IMF (Kroupa 2001) between $0.95 M_{\odot} < m_{1*} < 10 M_{\odot}$ and secondary masses are set by $m_2 = q m_1$, where q is uniformly distributed between 0 and 1. We discard binaries with $m_{2*} < 0.5 M_{\odot}$ as lower mass secondaries will not form DWDs within a Hubble time. With this condition, more than 90 per cent of the systems are discarded, saving significant computing time. We keep track of the number \bar{N}_b and mass \bar{M}_b of discarded binaries in order to normalize the number of DWDs to the stellar mass in our galaxy simulation (see Section 2.3).

We perform the population synthesis on $N_b = 2.5$ million systems per metallicity bin. We performed convergence tests on the period distribution of DWDs at their formation and determined that 2.5 million binaries *within the narrow mass range for the primary and secondary where DWD formation is possible*, is necessary to appropriately sample the tightest orbital periods. The latter have the highest GW frequency and will be very loud sources for *LISA*.

We use BSE to evolve our population forward up to the current age of the universe, tracking the systems that form binary white dwarfs. We use the following binary evolution parameters and characteristics for our population synthesis:

- (i) Tidal circularization is enabled.
- (ii) The Helium star mass loss factor is 1.
- (iii) Globally, the stellar wind speed is set with the parameter $\beta = 1/8$, following Hurley, Tout & Pols (2002a). Mass-loss for the most massive stars is set by Vink, de Koter & Lamers (2001). The latter is only relevant for progenitors of ONe WD.
- (iv) We use the parametrization by Claeys et al. (2014) to determine the envelope structure parameter λ for the common envelope.
- (v) We follow the common envelope evolution description from Tout et al. (1997) with efficiency parameter α set to 1 (see Ivanova et al. 2013). The critical mass ratio to start a common envelope interaction is set by the polytrope solution by Tout et al. (1997) depending on the mass and radius of the star, and set to 0.25 for stars in the Hertzsprung gap.
- (vi) We assume Roche lobe overflow mass transfer is conservative.
- (vii) Accretion on to a compact object has an efficiency of 0.5.
- (viii) We set the Eddington limit for mass transfer to 1.
- (ix) The mass of the WD at formation is naturally set by the competition between core-mass growth and envelope mass loss.

Once the DWD binary is formed, we assume its evolution is only determined by GW emission. As such, systems born with short orbital periods merge before the present day and we remove them

from our sample. Depending on the masses of the systems, such mergers may lead to type Ia supernovae (Iben & Tutukov 1984) or other transients (Saio & Nomoto 2004; Shen et al. 2012).

In some binaries, mass transfer may occur before the merger if at least one star fills its Roche lobe. For He–He DWDs, which have the largest radii, this typically occurs for periods below 3 min. The resulting mass transfer is unstable if the mass ratio of the binary $M_{\text{donor}}/M_{\text{accretor}} > 2/3$, leading to a fast merger (Marsh et al. 2004). This means that all He–He and CO–CO DWDs will merge quickly, potentially on faster time-scales than the GW emission predicts. The fate of binaries with smaller mass ratios (typically He–CO binaries) is less clear, the stability of the mass transfer depends on the spin–orbit coupling of the binary and the geometry of the accretion stream. Stable mass transfer could then lead to the widening of the orbit, which would keep the system in the *LISA* band for longer (Gokhale et al. 2007; Marsh 2011; Kremer et al. 2017). Such systems would appear like AMCVn systems due to the presence of the accretion disc. We choose not to model these systems, and any other type of AMCVn system. According to Brown et al. (2016c) most of these systems actually merge quickly, based on a study of the period distribution of a sample of Extremely Low Mass DWDs (ELM; Brown et al. 2010b, 2016a), and only a small fraction becomes an AMCVn binary. This was also predicted by Shen (2015) who proposed that even accreting double WD binaries with extreme mass ratios will merge due to classical nova-like outbursts on the accretor.

There are many important uncertainties, especially for the impact of mass transfer. In this work, we have chosen standard values for the binary and stellar evolution. As our focus is the combination with an updated model for the Milky Way rather than binary evolution, we restrict ourselves to this single set of parameters and leave a wider exploration for further work.

For each metallicity, we eventually produce a list of DWDs with their formation time after the formation of the progenitor binary, their orbital properties and masses. With 2.5 million initial binaries in a the appropriate mass range $\{0.95 M_{\odot} < m_{1*} < 10 M_{\odot}, m_{2*} > 0.5 M_{\odot}\}$, we end up with about 700 000 DWDs in each metallicity bin. For a binary fraction of 0.5 we find a DWD formation rate of 0.012–0.016 DWDs per unit Solar mass of total star formation (including binaries and singles). There is limited variation with metallicity.

We identify He (helium) WDs, CO (carbon/oxygen) WDs, and ONe (oxygen/neon) WDs separately. These different populations stem from different progenitor masses and/or binary evolution channels. Different subtypes of WDs have different radii and cooling times, which is important for their EM properties. In this paper we will show that different subtypes also contribute differently to the GW signal.

Fig. 1 shows the masses and orbital periods at the formation of the DWD binary as computed by BSE for an initial population at Solar metallicity. In comparison, Fig. 2 shows the properties of the corresponding progenitor binaries. The first column in Table 1 shows the absolute numbers of DWDs created in BSE. We distinguish four types of binaries depending on the nature of its white dwarf components:

(i) He–He WDs: These come from two low-mass stars, which evolve very slowly, and have both their envelopes stripped by common envelope interactions. He–He DWDs stem from binaries with short initial periods (or high eccentricities allowing for short periastron passages) and constitute a small fraction of the total population of DWDs, but they are important for *LISA*. The formation

time of these binaries is rather constant between 2 and 13 Gyr, which is much longer than the other channels. This results in low-mass WDs ($M_{\text{WD}} < 0.45 M_{\odot}$) in a very tight orbit. The tightest binaries are going to merge quickly due to their GW emission. They are also going to interact tidally during later phases, because of their comparatively large radius.

(ii) CO–CO WDs: These systems come from initially wider orbits, preventing the stripping of the envelope before the beginning of core He burning, and resulting in CO cores. Most of these systems have never interacted and will always have a large separation, which makes them less relevant for *LISA*. CO–CO binaries form in less than a Gyr and make up the bulk of the DWD population, with masses above $0.45 M_{\odot}$ (and often above $0.65 M_{\odot}$) and periods down to 1 h.

(iii) He–CO WDs: These systems are a mixture of both previous categories. They need about 2 Gyr to form and have low chirp masses because of their unequal masses. They can also form very tight DWDs and, combined with the He–He WDs, they are the most numerous in the *LISA* band although they make up only 10 per cent of the global DWD population.

(iv) ONe WDs: These are systems with at least one ONe WD, meaning that one of the stars has started carbon burning in the core before turning into a WD. As such, these WDs stem from massive stars: they form on short time-scales, come from initially well-separated stars (to prevent stellar mergers) and are rare.

In this paper, we will consider each population separately as they have different GW properties and we will show they also stem from different stellar populations.

2.3 Combined binary model and galaxy model

Each star particle within $\simeq 300$ kpc (roughly the virial radius of the Milky Way at $z = 0$) gets assigned n_{DWD} white dwarf binaries, depending its stellar mass at birth M_* and its metallicity (although the impact of metallicity is limited). We have

$$n_{\text{DWD}} = \frac{M_*}{M_{\text{tot,BPS}}} N_{\text{DWD,BPS}}, \quad (1)$$

where $N_{\text{DWD,BPS}}$ is the number of DWDs formed in a given binary population synthesis model resulting from an initial stellar population of total stellar mass $M_{\text{tot,BPS}}$ (see column 1 in Table 1). We only model N_b binary systems with primary and secondary masses allowing them to form DWDs, representing a stellar mass of M_b . Although we reject \bar{N}_b other binaries for the DWD modelling, their mass \bar{M}_b should count towards $M_{\text{tot,BPS}}$. Assuming a binary fraction $f_b = 0.5$, $M_{\text{tot,BPS}}$ should also account for a total number of $N_b + \bar{N}_b$ single systems, which are drawn for a complete Kroupa IMF (between 0.1 and $100 M_{\odot}$). In total, the equivalent stellar mass we model is given by

$$M_{\text{tot,BPS}} = \frac{1 - f_b}{f_b} \sum^{N_b + \bar{N}_b} m_1 + \frac{f_b}{f_b} \sum^{N_b + \bar{N}_b} m_1 + m_2. \quad (2)$$

As such, our subsample of 2.5 million binaries represent a total stellar mass of roughly $5.1 \cdot 10^7 M_{\odot}$. This number is identical for all metallicity bins we consider.

All the DWDs are stored in a dataframe. We randomly draw with replacement n_{DWD} from our BPS model for each star particle and add them to the dataframe. The DWDs inherit the formation time and metallicity of the progenitor star as well as its current position and position at formation. The formation time of the DWD is the sum of the formation time of the progenitor and of the DWD. DWDs

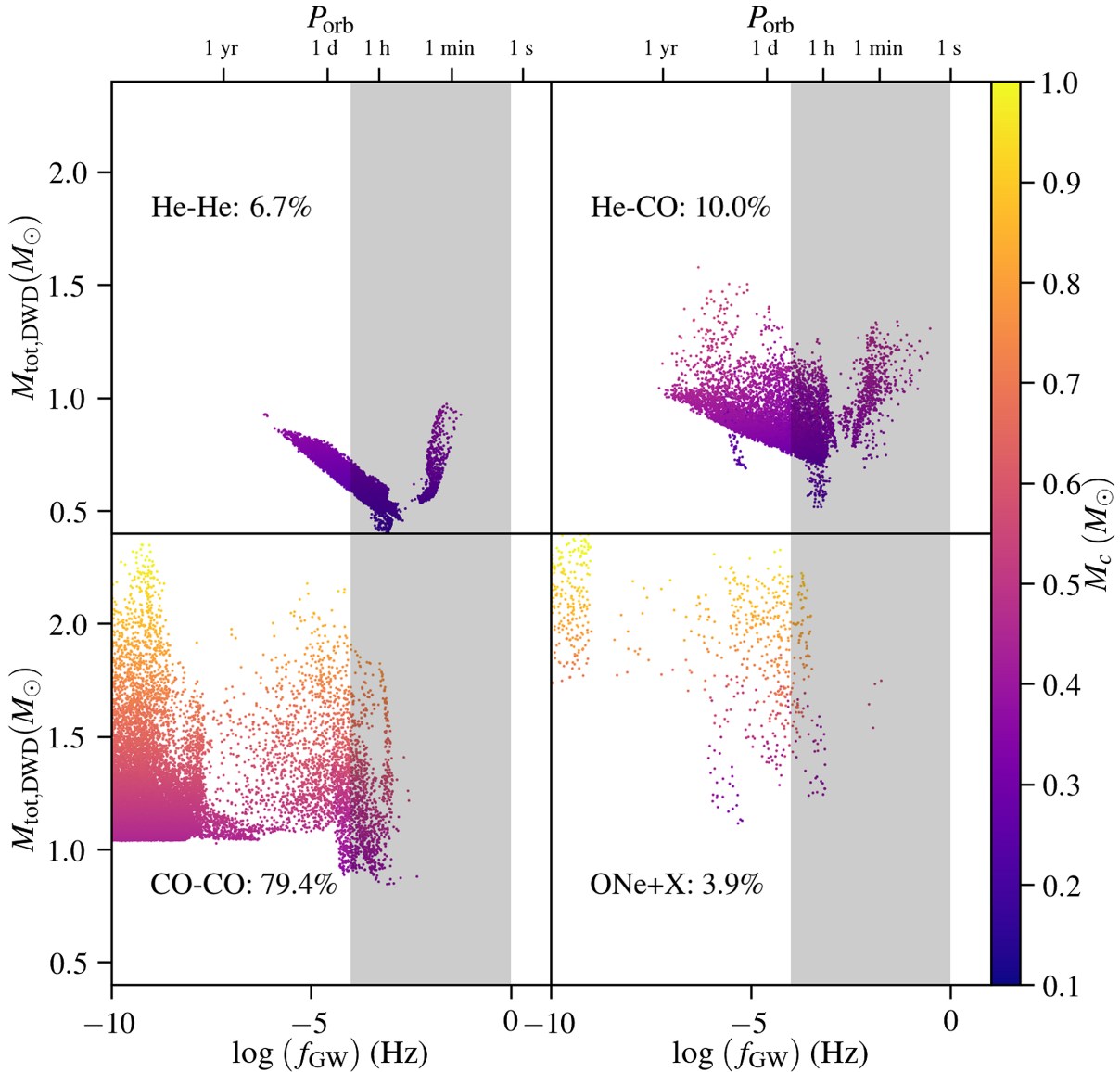


Figure 1. Periods at formation of the DWD binary and masses for a binary evolution model with 2.5 million binaries for $Z = Z_{\odot}$. Each quadrant shows a different subtype of resulting DWDs and the fraction of systems formed. We show the gravitational wave frequency f_{GW} and orbital period P_{orb} at the formation of the binary and its total mass $M_{\text{tot,DWD}}$. The colour shows the chirp mass $M_c = (M_1 M_2)^{3/5}/(M_1 + M_2)^{1/5}$ which is relevant for detectability with *LISA*. The grey vertical band shows the frequency range where *LISA* will be sensitive.

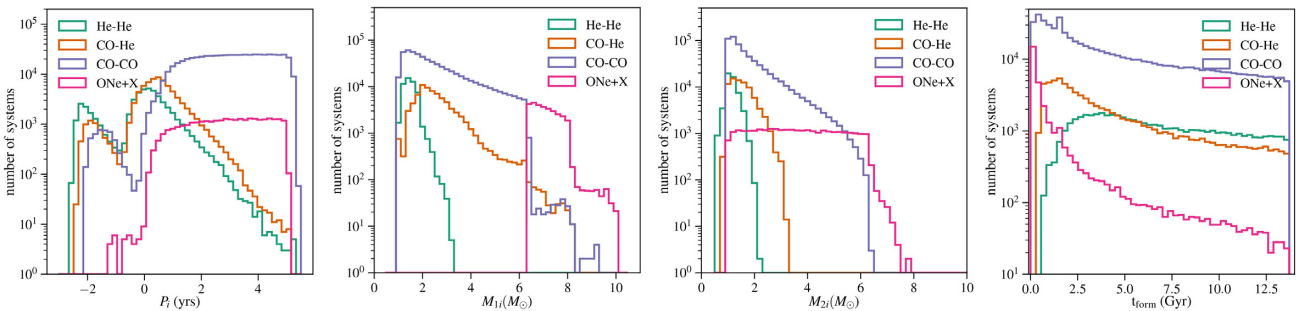


Figure 2. Initial stellar binary period (left) and progenitor masses (middle) of the final DWDs as a function of the DWD subtype for $Z = Z_{\odot}$. The right-hand panel shows the time needed to form the DWD.

Table 1. Summary of the main properties of the different types of DWDs. Columns are numbered at the bottom. From left to right, we specify the approximate number of systems formed in the binary population model (initial population of 2.5 million systems at Solar metallicity, see Section 2.2), the corresponding present-day Galactic population and the number of systems $f_{\text{GW}} > 10^{-4}$ Hz. Then we show the number of individually resolved systems, the number of well-localized systems and the number of systems with chirp mass measured within 10 per cent, for 2, 4, and 8 yr of observations. We indicate the total number as well as the fraction of each subtype.

	$n_{\text{DWD,BPS}}$	Galaxy model	$f_{\text{GW}} > 10^{-4}$	Resolved with <i>LISA</i>				Well localized				Measured mass		
				2 yr	4 yr	8 yr	2 yr	4 yr	8 yr	2 yr	4 yr	2 yr	4 yr	8 yr
He-He	51 500	9.7×10^6	1.9×10^7	1900	3500	5900	60	200	450	0	10	400		
	7 per cent	2 per cent	31 per cent	26 per cent	31 per cent	31 per cent	6 per cent	12 per cent	16 per cent	0 per cent	1 per cent	13 per cent		
He-CO	72 000	2.9×10^7	2.5×10^7	3600	5600	8600	500	1000	1700	100	600	1700		
	10 per cent	6 per cent	40 per cent	51 per cent	48 per cent	46 per cent	58 per cent	59 per cent	59 per cent	49 per cent	62 per cent	60 per cent		
CO-CO	609 000	4.4×10^8	1.2×10^7	1400	2200	3400	300	500	600	100	300	650		
	80 per cent	87 per cent	19 per cent	19 per cent	18 per cent	18 per cent	31 per cent	26 per cent	22 per cent	42 per cent	32 per cent	24 per cent		
ONe+X	30 000	3.1×10^7	5.8×10^6	200	350	800	40	50	90	20	40	90		
	4 per cent	6 per cent	9 per cent	3 per cent	3 per cent	4 per cent	4 per cent	3 per cent	4 per cent	9 per cent	4 per cent	3 per cent		
Total	763 000	5.1×10^8	6.2×10^7	7000	12000	19000	900	1800	2800	200	1000	2800		
	1	2	3	4	5	6	7	8	9	10	11	12		

with formation times beyond the present day are removed (about 50 per cent of the initial sample). We forward model the binaries until the present day via gravitational wave radiation, gradually shortening the orbit. We remove binaries that have already merged. Globally, less than 5 per cent of all the DWDs that were formed have merged by now. About 8 per cent of the He-He DWDs and 40 per cent of the He-CO DWDs have merged. About one per cent of the other binaries have merged by now. If the binary has not merged yet, its semimajor axis a and eccentricity e , which determine its GW emission, evolve according to (Peters & Mathews 1963)

$$\begin{aligned} \frac{de}{dt} &= -\frac{304}{15} \frac{G^3 \mu (M_1 + M_2)^2}{c^5 a^4} \frac{1}{(1 - e^2)^{5/2}} \left(1 + \frac{121}{304} e^2 \right) \\ \frac{da}{dt} &= -\frac{64}{5} \frac{G^3 \mu (M_1 + M_2)^2}{c^5 a^3} \frac{1}{(1 - e^2)^{7/2}} \left(1 + \frac{73}{24} e^2 + \frac{37}{96} e^4 \right), \end{aligned} \quad (3)$$

where μ is the reduced mass of the system. Typically one star particle generates 70–80 DWDs. To avoid spurious spatial clustering, we distribute the DWDs associated with each star particle relative to the particle's position using a spherical Epanenchnikov (quadratic) kernel whose length is determined adaptively based on the Mahalanobis distance to the ~ 10 nearest neighbouring star particles, using the EnLink algorithm described in Sharma & Johnston (2009).

Given our initial sample of DWDs, each DWD typically gets chosen for random assignment to a star particle about 200 times over the roughly 10 million star particles, with different positions and ages, representing the simulated Galaxy. This combination guarantees that the final catalogue of DWDs is only composed of truly unique binaries.

2.4 Modelling the gravitational wave emission

To estimate the capability of *LISA* to detect and characterize white dwarf binaries in the Galaxy models, we simulate the *LISA* data by co-adding the gravitational waveforms from all binaries with signals in the measurement band using the fast waveform generator in Cornish & Littenberg (2007). Without replicating the derivation, it is valuable to point out here that the dimensionless GW strain from a compact binary at a distance r is given by

$$h = 2(4\pi)^2 f_{\text{GW}}^{2/3} \frac{G^{5/3}}{c^4} \frac{M_{\text{c}}^{5/3}}{r}. \quad (4)$$

The measurement of the GW strain and frequency alone are insufficient to determine the chirp mass of the binary, which is degenerate with the distance. The chirp mass (and therefore distance) can be determined for Galactic binaries in the *LISA* band, having wide orbital separations and orbital velocities $\ll c$, to leading order in the frequency evolution

$$M_{\text{c}} = \frac{c^3}{G} \left(\frac{5}{96} \pi^{-8/3} f_{\text{GW}}^{-11/3} \dot{f}_{\text{GW}} \right)^{3/5} \quad (5)$$

assuming that other contributions to the orbital period evolution (e.g. mass transfer, tides, etc.) are sub-dominant effects. Note that \dot{f}_{GW} is a difficult parameter for *LISA* to constrain, so chirp mass measurements are only possible for ‘outliers’ of the total population, requiring high signal-to-noise (S/N), comparatively large \dot{f} , and/or long integration times for the *LISA* observations. Fortunately, due to the large number of detectable binaries, even the tails of the source distribution are well populated.

Our simulated *LISA* response to the Galaxy models use spacecraft noise levels and orbits consistent with those in the *LISA* mission proposal (Amaro-Seoane et al. 2017). Determining which of the simulated binaries are individually resolvable is challenging in the regime where the confusion noise dominates the data stream. From the full input binary population, the detectable sources are identified by using an iterative process that utilizes a median smoothing of the power spectrum to estimate the noise level (dominated by source confusion around 1 mHz), regresses binaries from the data with signal-to-noise ratios $S/N > 7$ as detected sources, and cycles until the detection ‘catalogue’ converges (Timpano, Rubbo & Cornish 2006; Nissanke et al. 2012). This approximate method is in qualitative agreement with more realistic search strategies (Crowder & Cornish 2007; Littenberg 2011)

For the detected binaries, we assume Gaussian measurement uncertainties centred on the true parameters for each source, completely characterized by the covariance matrix. To compute the inverse covariance matrix we use the Fisher approximation, with a central differencing numerical differentiation scheme to calculate derivatives of the waveforms (Cutler & Flanagan 1994). The Fisher matrix is only an approximation with well-publicized shortcomings (Vallisneri 2008) but, similar to the argument for the hierarchical search method, a more robust error analysis (e.g. using stochastic sampling methods) requires prohibitive computationally resources for the scope of this work. Furthermore, where the Fisher approximation is most accurate is in the high S/N regime, and many of the results in this work are focused on exactly those

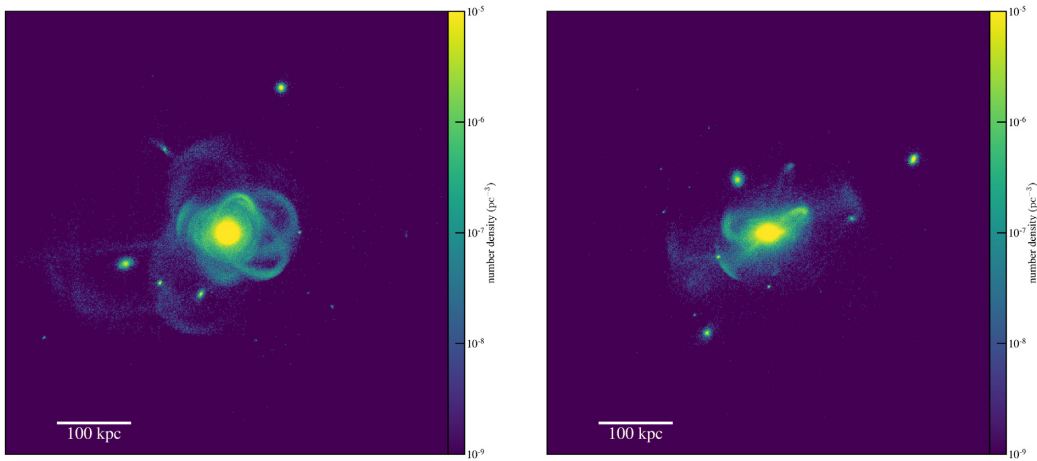


Figure 3. Large-scale maps of the surface density of the number of DWDs in the simulation, viewed faced on (left) and edge-on (right). To zeroth order, the spatial distribution is very similar to the stellar distribution (not shown). The main galaxy shows a disc, bulge, and stellar halo. DWDs are also present in the tidal streams and satellite galaxies.

binaries because they are the systems that yield the best parameter constraints.

The computation of the GW signal is only performed for the binaries with present-day frequency above 10^{-5} Hz.

3 RESULTS

3.1 Origin of different populations of short-period DWDs in the Milky Way

Here we describe the properties of the tight DWD binaries in an Milky Way like galaxy based on the combination of the cosmological simulation and the binary population synthesis model. We will describe how different DWD populations arise from the global stellar population and vice versa.

The second column in Table 1 shows the total numbers of the DWDs in and around our MW-like galaxy. About 500 million systems have formed, most of them at very wide orbits. In comparison with the direct output from the binary evolution model (which assumes a unique burst of star formation) we find that He–He and He–CO DWDs are under-represented in the Galaxy model. This is because many of these DWDs form at high frequencies, and many have merged by the present day. Additionally, for the He–He DWDs, the formation time is comparatively longer, which means the recently formed stars cannot have contributed to this population. Of the 500 million binaries in the MW, most of them are too separated to have ever interacted. In the remainder of this paper, we will only focus on binaries that are relevant for *LISA*.

The third column in Table 1 shows the number of systems with a $f_{\text{GW}} > 10^{-4}$ Hz. There are roughly 60 million systems in our simulation, which is consistent with previous results (e.g. Nelemans et al. 2001b; Ruiter et al. 2010; Nissanke et al. 2012). He–He and He–CO DWDs are over-represented at these high frequencies (respectively 31 and 40 per cent) because they have undergone two common-envelope phases. Fig. 3 shows the surface density of the short-period binaries in and around the galaxy, with and edge-on and face-on view. Overall, the distribution is similar to the stellar distribution (not shown here). As our Galaxy model is based on a cosmological simulation, the DWDs are naturally present in all the components of the Milky Way such as the thin and thick disc, the bulge, the stellar halo, tidal streams and satellite galaxies. This

is different from all previous models where the spatial distribution is a parametrized, symmetrical model of the discs and bulge (and sometimes the stellar halo, as in Ruiter et al. (2010)).

Fig. 4 shows a histogram of the radial distance with respect to the Galactic centre (left) and the distance above the plane (right) of the binaries. Globally, the DWD distribution follows the stellar distribution, although DWDs somewhat prefer the bulge, stellar halo and satellites and are less present in the disc. This effect is mostly visible for CO–He DWDs and even more He–He DWDs, which become more numerous than the CO–CO DWDs outside of the disc. On the contrary, the DWDs stemming from the most recent stars, such as CO–CO and ONe–X DWDs slightly prefer the disc. This trend is confirmed in the other cosmological simulations we analysed. These distributions can be explained by the minimal stellar age of each population (see Fig. 2).

When focusing only on the highest frequency systems shown with thin lines ($f_{\text{GW}} > 10^{-3}$ Hz, where most of the individually resolved sources for *LISA* will be found), we find that they more closely follow the stellar distribution than their low-frequency counterparts. Still, they keep distinct spatial distributions, as is shown in Fig. 5. These maps show the galaxy edge-on: the He–He DWDs distribution is almost spherical due to the bulge and halo, with a thick disc. On the opposite, the CO–CO DWDs are present almost exclusively in a very thin and elongated disc. The He–CO DWDs present an intermediate distribution, with prominent disc, although with a smaller scale height than for He–He DWDs, and a limited contribution from the bulge and halo.

A more complete understanding of the present-day DWD population in an MW-like galaxy comes from the formation time of their progenitor stars. Fig. 6 shows that the formation of DWD progenitors follows the global star formation rate until $z \simeq 1$ where it starts declining. This is related to the typical formation time of 2 Gyr for a CO–He DWD and beyond 5 Gyr for a He–He DWD. Conversely CO–CO and Ne–X DWDs can form on a much shorter time-scale and trace their progenitors star formation history almost completely. For the high frequency systems, only young DWDs are present, so the contribution increases towards recently formed progenitors, except for the He–He DWDs. Again, the different behaviour for He–He DWDs is the wider range of the duration of stellar evolution. A He–CO, CO–CO, or ONe–X DWD detected with high frequency probably stems from a progenitor formed less

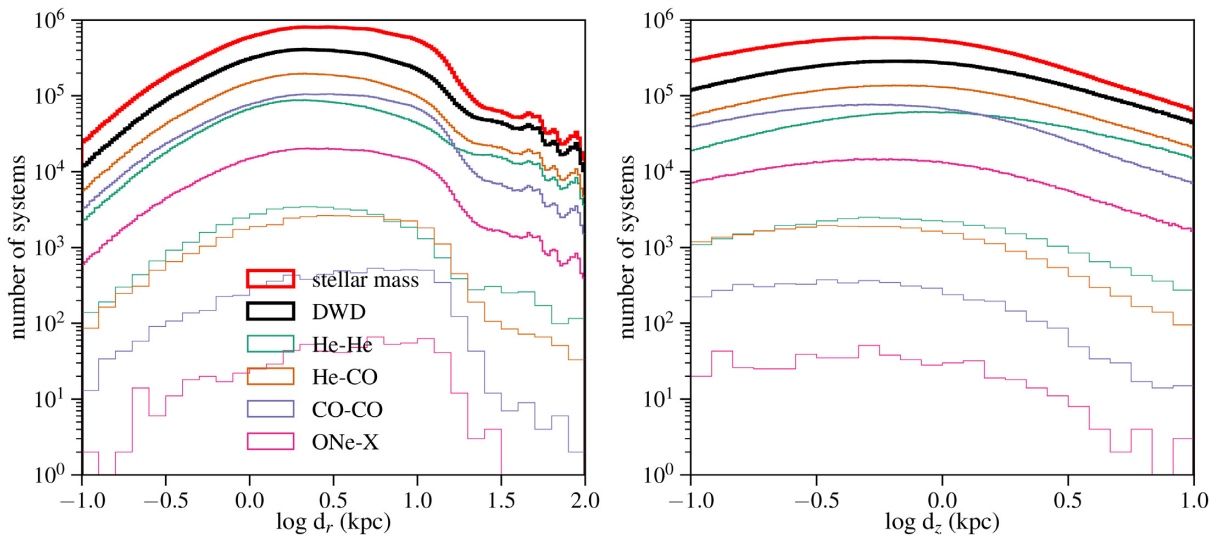


Figure 4. Spatial distributions of the DWDs (black) in comparison with the stellar mass (red, rescaled by a factor 1000). Different colours show different subtypes, and the thin lines only show the binaries with $f_{\text{GW}} > 10^{-3}$ Hz. Both plots have the same legend.

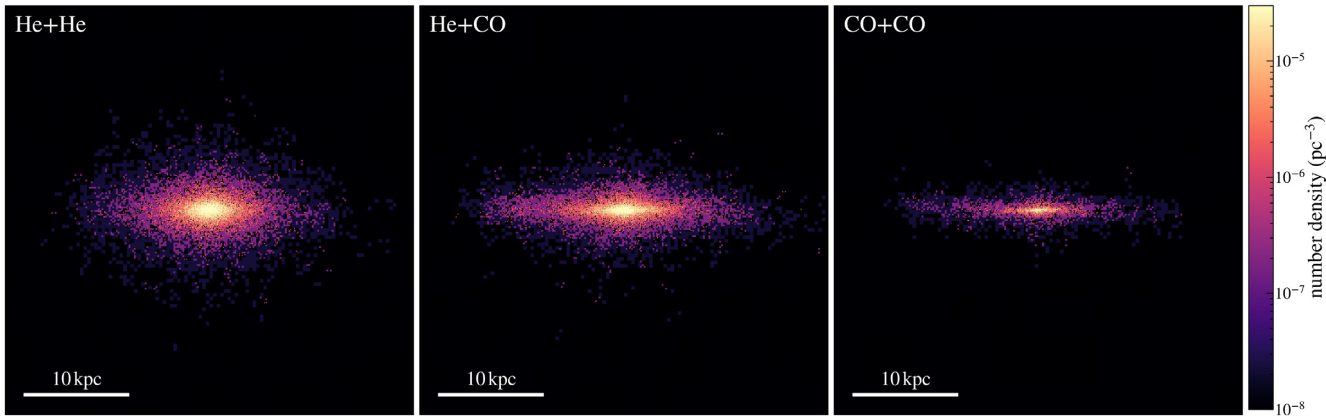


Figure 5. Maps of the He–He DWDs (left), He–CO (middle), and CO–CO DWDs (right) viewed and edge-on. These maps only show the binaries with $f_{\text{GW}} > 10^{-3}$ Hz, which are the most likely to be individually resolved by *LISA*. We do not show the Ne + X binaries due to their sparcity. Their distribution is very similar to the COCO binaries.

than 2 Gyr ago ($z \lesssim 0.2$), while a He–He DWD progenitors likely formed between 3.5 and 6 Gyr ago. These effects explain the different spatial distributions shown in Fig. 5. As the metallicity of the Galaxy globally increases with time, we find that CO–CO and ONe–X DWDs stem from stars with the same metallicity distribution as the global stellar population, peaking around $Z = 3Z_{\odot}$ while the He–He DWDs mostly stem from stars with lower metallicity (peaking around Z_{\odot}).

3.2 Prospects for detecting short-period DWDs in the Milky Way

Here we discuss the frequency/orbital period distribution and distance to the Sun of the different binary populations. These are crucial aspects for detection with gravitational waves and/or EM observations. Fig. 7 shows the frequency distribution of all the binaries with $f_{\text{GW}} > 10^{-5}$ Hz. The middle panel, showing the present-day distribution, shows that the CO–He DWD population dominates below $\simeq 10^{-3}$ Hz and the He–He DWDs are slightly more numerous beyond that. The left-hand panel shows the binary

distribution at the their formation: initially roughly 90 million binaries were formed with $f_{\text{GW}} > 10^{-5}$ Hz, with their maximal frequency up to a few Hz. All the binaries with initial $f_{\text{GW}} > 10^{-2}$ Hz have merged by now. For binaries formed with $f_{\text{GW}} > 10^{-5}$ Hz, 40 per cent are still currently present, with 32 per cent, 44 per cent, 47 per cent, 20 per cent of the He–He, He–CO, CO–CO, ONe–X binaries still present, respectively. He–He and ONe–X DWDs undergo most of the mergers because of their tight initial orbits (for He–He DWDs) and their high chirp masses (for ONe–X DWDs). Note that we have not removed He–He binaries undergoing Roche lobe overflow from this sample (see Section 2.2). The latter would occur for $f_{\text{GW}} \gtrsim 11$ mHz, where the contribution of He–He DWDs is small. The overall low number of high-frequency CO–CO DWDs is due to their limited birth rate at high frequency (see shaded area in Fig. 1) combined with a merger time of a few tens of millions of years for systems initially formed with an orbital period of one hour. In comparison He–He DWDs with an initial period of an hour need about 100 Myr to merge. In all cases, the DWDs in high-frequency systems must have formed recently, otherwise they would have merged. Given the wide range of formation times of He–He DWDs,

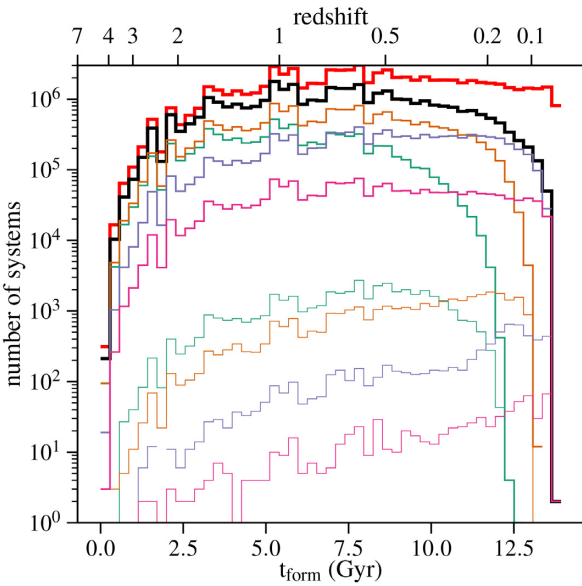


Figure 6. Formation time of the progenitors of the DWDs (black) in comparison with the stars (red, rescaled by a factor 1000). Different colours show different subtypes, and the thin lines only show the binaries with $f_{\text{GW}} > 10^{-3}$ Hz (colour scheme is identical to Fig. 4).

recent DWD formation does not imply that the progenitor binary formed recently.

The initial frequency distribution of the currently present DWD binaries right-hand panel shows that most of them initially had a frequency around 10^{-4} Hz and have hardened to their present-day orbital frequencies. Systems with initial frequency below $\simeq 5 \times 10^{-5}$ Hz have not evolved significantly since their formation. This implies that most DWD binaries, which are formed with a lower frequency, will never be relevant to *LISA*.

Fig. 8 shows the cumulative distribution of the DWDs within a certain distance to the Sun. CO–CO and He–CO binaries dominate at all distances. When focusing only on the highest frequency systems, CO–He DWDs are the most numerous within a few kpc, but there is a significant contribution of He–He and CO–CO DWDs as well. This is roughly the distance up to which *Gaia* will be able to observe verification binaries (Korol et al. 2017). Beyond $\simeq 5$ kpc, which will be observable by LSST, He–He and He–CO DWDs largely dominate the sample. In the following section we present the observable properties of the GW emission of our population.

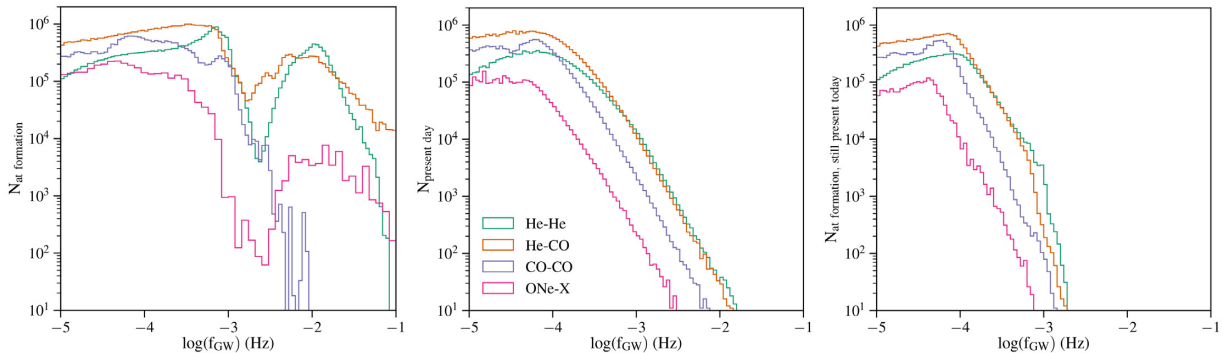


Figure 7. Distribution of the frequency of the DWD binary population with $f_{\text{GW}} > 10^{-5}$ Hz. The left plot shows the frequency of all the binaries at the formation of the DWDs. The middle plot shows the frequency of the present-day binaries (the binaries that have not merged yet). The right plot shows the initial frequency of the binaries which have not merged by the present day.

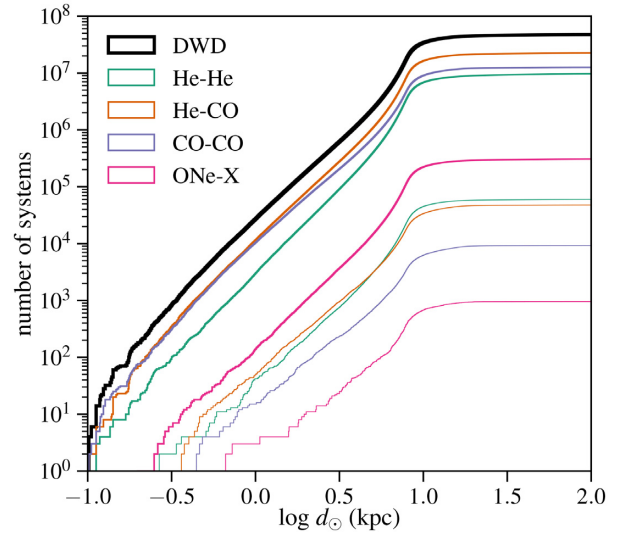


Figure 8. Cumulative distribution of the distance to the Sun of DWDs (black). Different colours show different subtypes, and the thin lines only show the binaries with $f_{\text{GW}} > 10^{-3}$ Hz.

4 GW SIGNATURES

In this section we predict the detections of the short-period DWDs with *LISA*, based on the complete GW emission model described in Section 2.4. We explain how the binaries described in Section 3.2 are affected by *LISA*'s response function. We present the properties of the individually resolved sources (Section 4.1), including implications of mass and distance measurements as well as sky localization. As our method includes a cosmological model of the Galaxy, we detail the possibility to detect and identify sources in the stellar halo, stellar streams and satellites (Section 4.2).

4.1 Individually resolved sources

Columns 4–6 in Table 1 summarize the number of sources individually resolved by *LISA* over time. A source is considered to be resolved if it can be uniquely identified within its frequency bin, with an S/N of at least 7. Contrary to (most) EM detections, this definition of a source does not have any implication on our ability to localize it on the sky. We find roughly 12 000 resolved binaries after a 4-yr mission.

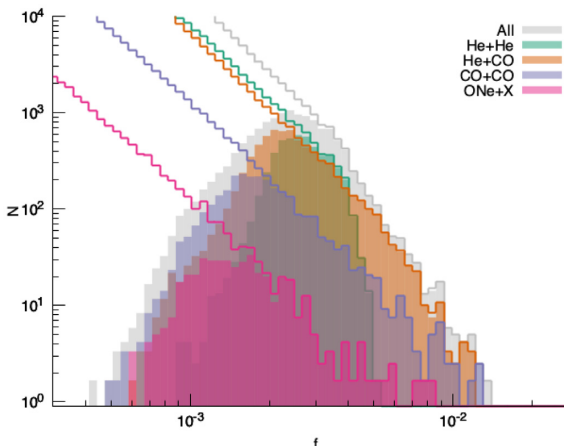


Figure 9. Frequency distribution of the systems with $S/N > 7$ in comparison with the total distribution after an 8 yr observing time. Note that the catalogue of detected binaries with $f_{\text{GW}} \gtrsim 3 \text{ mHz}$ ($f_{\text{GW}} \gtrsim 2 \text{ mHz}$ for the more massive UCBs) is complete.

The comparison between the resolved population (solid histogram in Fig. 9) and the complete DWD population in the Galaxy (coloured lines) highlights that the sample of resolved binaries is complete down to 3 mHz, and even 2 mHz for the most massive binaries. Effectively, any binary with a period below 15 min will be individually resolvable, no matter its location in our Galaxy, including the nearby satellites. As such, all the detections of these systems will be crucial to constrain binary evolution.

Fig. 9 shows the histogram of the frequency of the different types of binaries detected by *LISA*. This plot directly shows how the global frequency distribution in Fig. 7 translates into *LISA* detections. Additionally, we have manually removed binaries which may be undergoing Roche lobe overflow from the sample, as they have likely merged already (see end of Section 2.2). This effectively affects less than 5 per cent of the individually resolvable binaries. We find that He–CO DWDs and He–He DWDs are the most numerous in the *LISA* band and among the detected sources, even though their contribution to the global Galactic population is about 5 per cent at most. This is because these binaries typically have the tightest orbits. He–He DWDs are present only up to about 5 mHz, because He WD have the largest radii and Roche lobe overflow happens.

Fig. 10 shows the contribution of the individually resolved systems of each type of binary to the GW signal. These maps show the same frequency dependence as Fig. 9. The GW amplitude is set by the distance to the source, the frequency of the binary and the chirp mass (equation 4). The He–He systems are very numerous but have the lowest GW amplitude due to the lower chirp mass, followed by the He–CO systems. Conversely the CO–CO and ONe–X systems are less numerous but contribute at higher amplitudes.

Naturally the number of detected systems will increase over time as signal is accumulated and more and more systems become detectable above the instrumental and confusion noise. The different columns in Table 1 emphasize that particularly the He–He DWDs will mostly benefit from an extended mission. After the nominal mission of 4 yr, a third of the newly detected systems will be He–He DWDs, as opposed to one quarter during the first 2 yr of the mission. This is due to the fact the He–He DWDs have a low GW amplitude (see Fig. 10) and a low frequency (see Fig. 7) which means that many of them will be buried in the foreground noise, which will decrease

as the number of resolved systems increases. The determination of the frequency of the systems will allow statistical studies of binary evolution.

For most of the sources, the measured frequency of the binary will be effectively constant during the observing time. For certain sources, *LISA* will also be able to measure the first frequency derivative f'_{GW} and determine both the chirp mass and distance of the binary (equations 4–5). This will only occur for chirping binaries, which frequency changes over the course of *LISA*'s lifetime: the systems with the highest masses and frequencies. Fig. 11 shows the binaries with chirp masses measured with better than 10 per cent uncertainty after an extended mission of 8 yr. Out of the $\simeq 3000$ systems the majority will be CO–CO ($\simeq 700$) and He–CO DWDs ($\simeq 1700$). The detailed numbers are provided in columns 10–12 of Table 1.

Given the complexity of stellar evolution, DWDs of a given subtype can have a wide range in chirp masses. This limits the classification of DWDs based on the chirp mass to a few hundred systems. This would probably also be quite dependent on the details of the binary model. The outcome of the different phases of mass transfer probably have the strongest influence on the final masses and periods (see e.g. Toonen, Nelemans & Portegies Zwart 2012; Toonen, Voss & Knigge 2014a). Unfortunately *LISA* will not be able to determine the component masses of DWDs, making the classification of the different binaries very uncertain and additional information from EM observations or theoretical models may be necessary.

Mass measurements become possible when a frequency derivative is measured. The latter really benefits from long integration times for the observations. Globally, during the first 2 yr, 200 systems will have mass measurements, the two following years will yield an additional $\simeq 750$ measurements and an extended mission would yield about 450 additional measurements per year. These values are crucial to characterize the systems and most of the statistics will be obtained with an extended mission. This is even more the case for He–He DWDs, which will only contribute to the mass measurements during an extended mission. The latter are ideal candidates for EM observations due to their large radii.

Sky localization and distance measurements are crucial to enable the identification of EM counterparts, based on existing data or new observations. A source is considered to be well localized if we can determine its position in the sky within 10 deg^2 and its distance within 50 per cent. These sources are the best candidates for EM follow-up or cross-matching with EM catalogues. Columns 7–9 in Table 1 indicate the number of well-localized systems in the simulation. Current large-scale sky surveys reach an average depth of $\approx 20\text{--}21$ mag which limits surveys to $\approx 1\text{--}2$ kpc. In a few years from now LSST will reach an average r -band depth of ≈ 24.5 mag in a single epoch and ≈ 27.5 mag in the co-added map (Ivezić et al. 2019) allowing us to detect the EM counterpart up to ≈ 5 and ≈ 10 kpc, respectively. Fig. 12 shows the expected number of systems with distance uncertainties of 50 per cent and sky localization better than 10 deg^2 , well matched to LSST's field of view. At the end of the nominal mission, a few hundred systems could have counterparts. With an extended mission and stacked LSST data, a few thousand systems could be found.

Fig. 13 shows the sky localization and its uncertainty for the different types of binaries. Measuring a sky localization within 10 deg^2 is aided by increased signal to noise, which accumulates throughout the mission for these sources. Precise sky localizations will typically be available only after 2 yr of the mission, or even after 4 yr for the fainter systems such the He–He. The sky maps

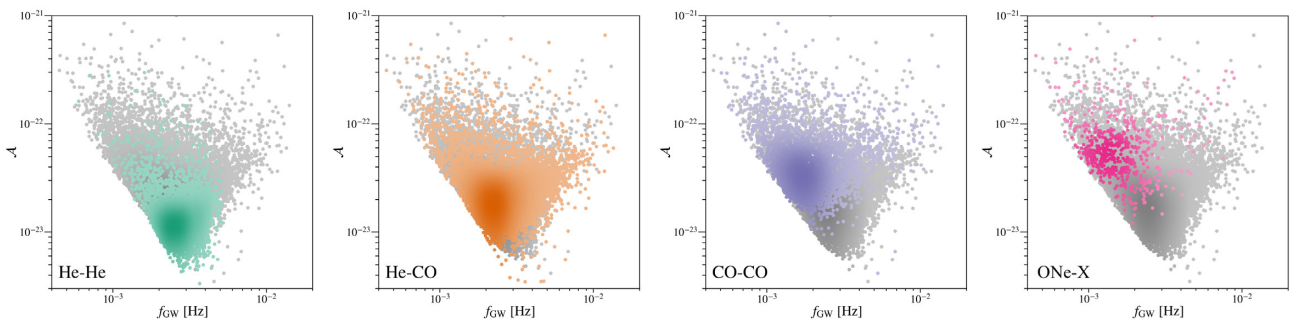


Figure 10. Heat maps of gravitational wave amplitude versus frequency for all the systems with $S/N \geq 7$. The colour schemes are linear and there is less than an order of magnitude difference between the brightest spots and the faintest.

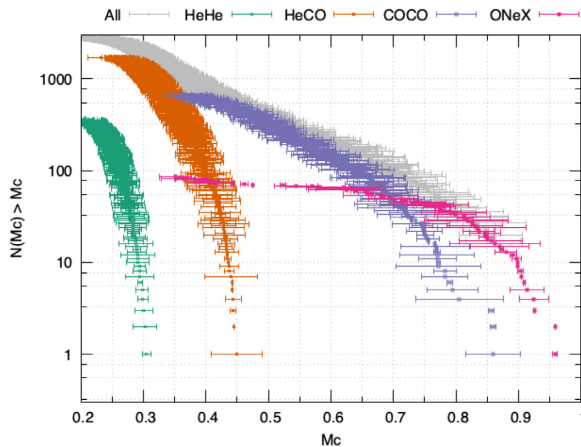


Figure 11. Number of binaries above a given chirp mass, with a well measured chirp mass, for each binary subtype. Each point shows an individual systems with chirp mass errors below 10 per cent, shown with the error bar. For this simulation (8 yr observing time) we can expect to unambiguously identify O(1000) He–CO DWDs, O(300) CO–CO DWDs, and O(10) ONe–X systems.

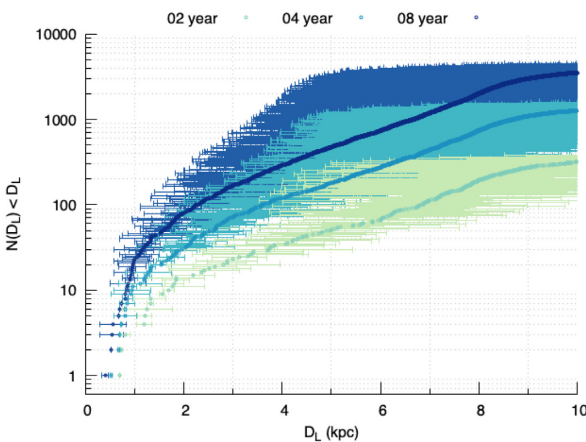


Figure 12. Distance measurements and their uncertainties of all the well-localized binaries within 10 kpc from the Sun after 2, 4, and 8 yr of the *LISA* mission.

confirm that *LISA* will detect DWDs throughout the Galaxy, with important contributions from the bulge and the thick disc. The He–He binaries, which are likely to have the brightest EM counterparts, are overwhelmingly present in the bulge, which will make them

very difficult targets due to the large distance and density of the sources.

4.2 Detection of systems in the stellar halo and beyond

Fig. 9 shows that all systems with $f_{GW} \geq 3$ mHz will be resolved. The latter include systems in the outskirts of the Galaxy, including satellite galaxies and streams. Yu & Jeffery (2010) and Ruiter et al. (2009) found that some DWDs located in the Galactic halo will contribute to the *LISA* detections. Korol et al. (2018) calculated that, given their stellar masses, the Magellanic Clouds and the Andromeda galaxies are likely to harbour binaries detectable by *LISA*, which may be our only way to constrain the Type Ia supernova rate in our neighbourhood. These studies do not determine whether we will be able to assign these systems to the Galactic halo, the Magellanic Clouds or Andromeda based solely on the GW detections.

In this section we determine whether *LISA* will detect any systems belonging to the stellar halo, and whether it will be able to properly identify them as such. Here we define the stellar halo as the ensemble of stars that are present within the virial radius of the main galaxy but were not formed in the main galaxy (*ex situ* star formation), although other works sometimes select on present-day distance or kinematics. These stars are typically 8–10 Gyr old. Our definition of the stellar halo therefore includes satellite galaxies, coherent stellar streams, and the phase mixed remnants of completely disrupted satellites. It does not include stars formed in the main galaxy that were perturbed on to more radial orbits. We directly use the information available from the simulation regarding the position of each star particle at birth to separate *in situ* (distance from host centre < 30 kpc at formation) from *ex situ* (> 30 kpc) stars.

In total we find that about 5 per cent of the resolved binaries are halo objects. In comparison 1 per cent of the stars in the simulations are halo objects, and DWDs are over-represented in the halo. Fig. 14 shows the localization of the so-called halo DWDs that have distance measurements with less than 50 per cent uncertainty after an extended mission (8 yr). Many of these DWDs are at small Galactocentric distances today such that they overlap spatially with *in situ* stars (though Brown et al. 2016b were able to select the halo objects thanks to their peculiar proper motions). A few of the halo binaries have measured distances beyond 50 kpc from the centre of the Galaxy (red dots) and are effectively located in satellite galaxies and streams. Fig. 15 shows the number of systems detected by *LISA* beyond a certain distance to the Sun. This figure shows the inverse of Fig. 12, which focused on systems *within* a certain distance. Fig. 15 shows that a handful of systems will effectively stand out from the global distance distribution, which falls off

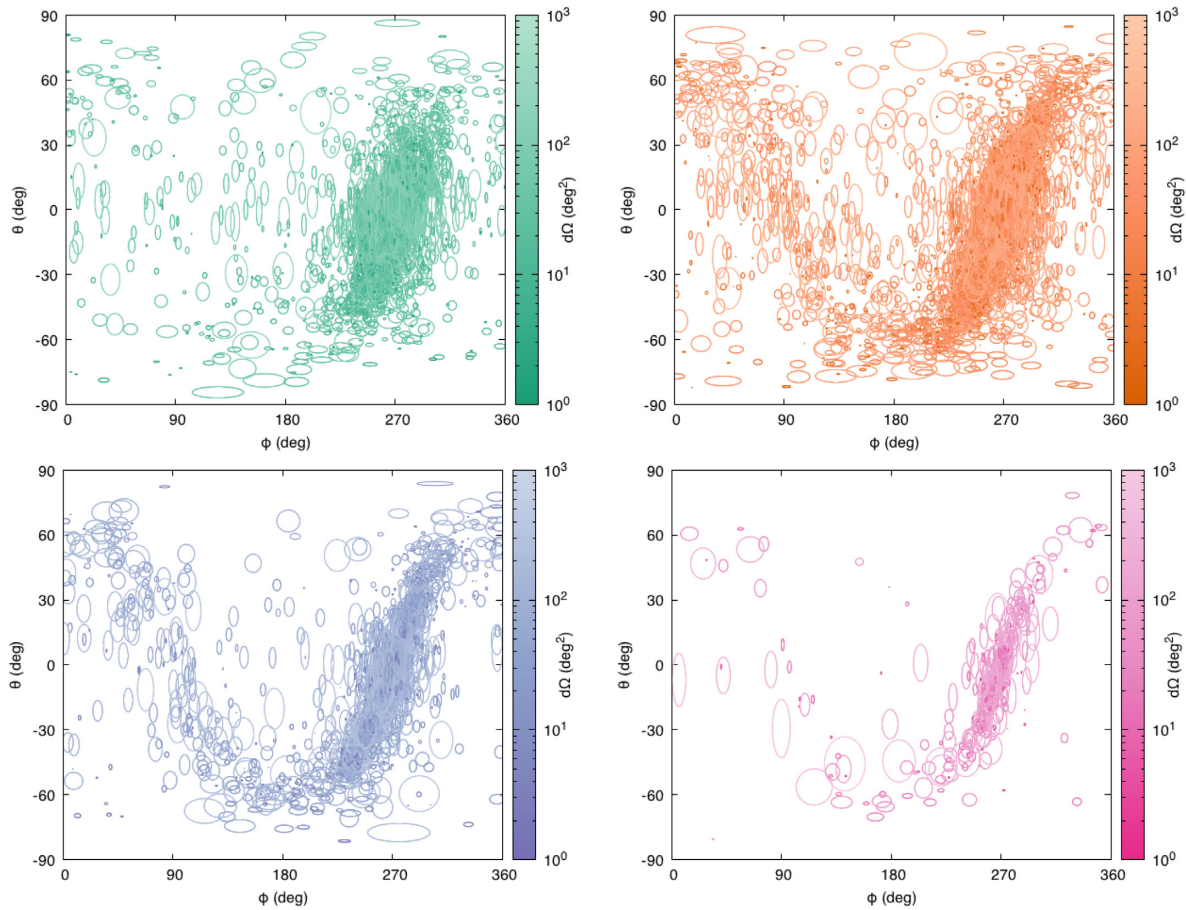


Figure 13. Sky localization in ecliptic coordinates for the well-localized binaries. The ellipses encompass the 1σ uncertainties on the inferred sky location, and the colour scale indicates the angular size of the error region in square degrees.

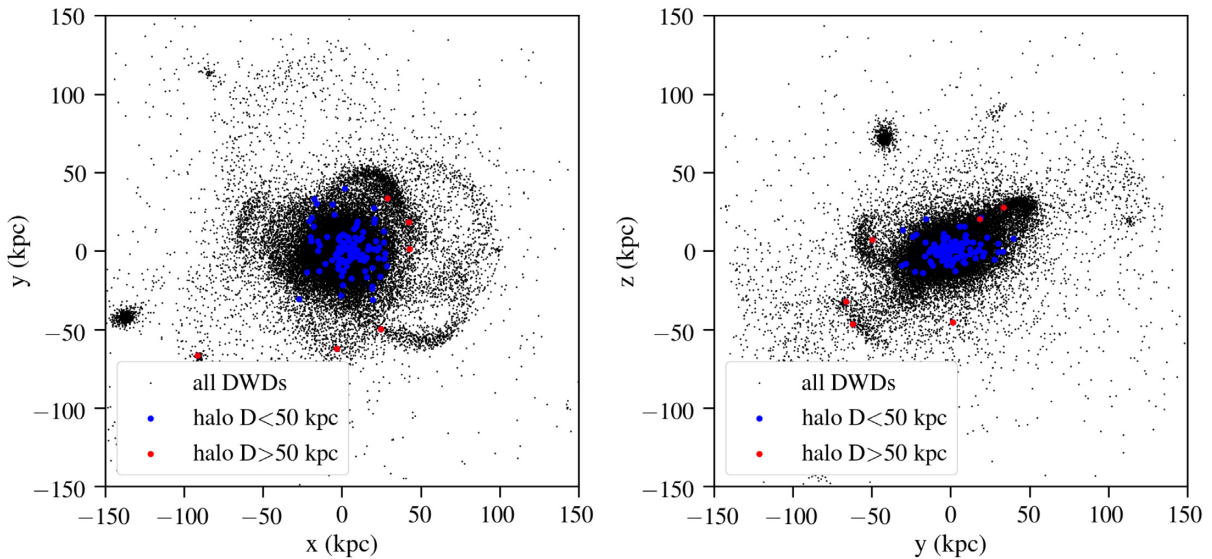


Figure 14. Distribution of DWDs which have formed outside of the main galaxy (blue dots) and have been accreted. A small fraction of these binaries (red dots) can be attributed to the stellar halo due to their large distance (galactocentric distance larger than 50 kpc), measured with less than 50 per cent accuracy. We show the distribution of DWDs with $f_{\text{GW}} > 10^{-5}$ Hz is shown in black downsampled by a factor 100 for readability, regardless of possible detectability.

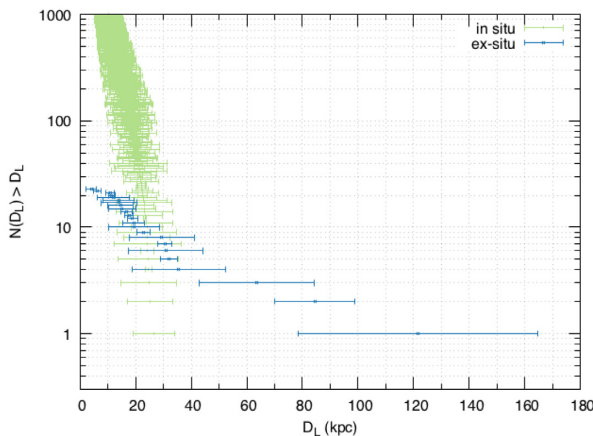


Figure 15. Number of binaries above a given distance, which have their distance determined to better than 50 per cent. Each point represents an individually resolved binary and the error bar along the x -axis shows the uncertainty range of the distance measurement. We distinguish between binaries formed in the main galaxy (*in situ* star formation, green) or in satellites (*ex situ* star formation, blue). For this simulation (8 yr observing time), a handful of the *ex situ* binaries have distance measurements which distinguish them from the other binaries and locate them in satellite galaxies and tidal streams.

sharply around 25 kpc. All these systems have formed outside of the Milky Way. This measurement will only become possible after an extended mission, when the uncertainties on the distance measurements become small enough to distinguish the distances of the halo objects from the distance distribution of systems from the main galaxy. These systems typically have sky localizations within $10\text{--}30 \text{ deg}^2$, which will probably be sufficient to assign them to a satellite galaxy.

The number of systems with well-measured distances does not depend on the randomly chosen localization of the Sun, within a ring located at 8.2 kpc from the Galactic centre. In other words, *LISA* will produce a complete catalogue down to a certain frequency, including the halo systems. However, contrary to the other results in this paper, the number of detected and well-localized halo binaries does depend on the cosmological simulation and its accretion history. Our simulation does not include massive satellite galaxies such as the Magellanic Clouds, which will likely host systems. We can safely speculate that the identification of halo objects around the Milky Way would be possible if the uncertainty of the distance measurement is reduced by more careful selection based on sky position and/or cross-matching with catalogues of satellite galaxies and streams.

5 DISCUSSION

Our model provides the first prediction of DWDs based on a binary population synthesis model combined with a cosmological simulation. The simulations produce self-consistent star formation in a cosmological volume. As such, our work mostly differs from previous models in its assumptions on the Galactic structure and star formation history. Importantly, our model does not rely on parametrized, axisymmetrical, models of the different components of the MW and self-consistently includes a stellar halo and satellites and streams.

Globally we find that our model predicts comparable numbers of DWDs and of detectable systems than previous studies (e.g.

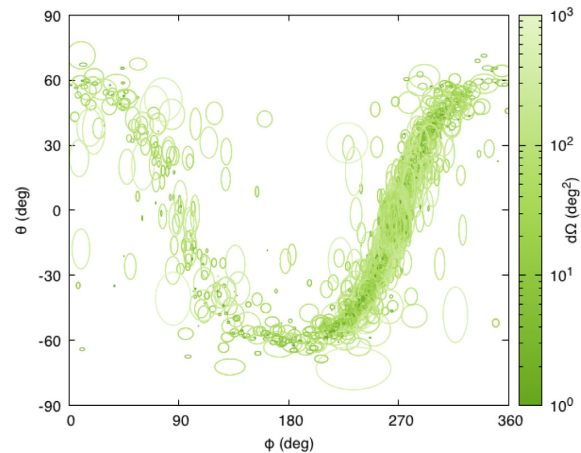


Figure 16. Sky localization of the individually detected DWDs assuming a spatial distribution following Nelemans et al. (2001b), after 8 yr of observations. The star formation history and binary evolution model is the same as the rest of the paper. This plot can be directly compared to the sum of the distributions presented in Fig. 13.

Nelemans et al. 2001b; Nissanke et al. 2012) although an exact comparison is impossible due to the different assumptions on the *LISA* mission (arm length, duration of the mission, and S/N threshold for detections) and binary evolution. Our analysis predicts fewer detectable and well-localized binaries than Korol et al. (2017) but also Cornish & Robson (2017) which sought to update the results of Nissanke et al. (2012) with the current *LISA* design. Part of this difference can be accounted for by a global higher star formation rate in the previous models, which naturally yields more white dwarf binaries. The remaining difference is likely caused by differences in the treatment of binary evolution, including a different choice of the stellar structure parameter λ . A complete study of the impact of the different parameters (and their uncertainties) on the final binary population is beyond the scope of this paper.

The importance of our model lies in its assumptions (or lack thereof) on the Galactic structure and typical ages for different stellar populations. Fig. 16 shows the spatial distribution of the systems detected by *LISA* with the Galactic model used in Nelemans et al. (2001b). All other aspects of the model (global metallicity and star formation history and binary evolution) are identical to the model presented here. In comparison with our model shown in Fig. 13 this model shows a very thin and well-defined disc, a small bulge and no stellar halo. Quantitatively, the analytic models predict five times more systems in the innermost kpc of the Galaxy and about an order of magnitude less beyond 10 kpc. There are almost no detections outside the plane of the disc. Although the localization of the binaries is different from our model, the global numbers of resolved and well-localized systems is comparable similar to ours. This is probably related to the completeness of the *LISA* detections down to a few mHz. Importantly, the simplified model cannot predict the different spatial distributions of the different types of binaries, and its impact on multimessenger astronomy.

Ruiter et al. (2009) specifically studied the detection of DWDs in the Galactic halo and compute that its signal is a factor 10 lower than the disc's signal. We find somewhat smaller numbers and confirm that He–He systems dominate in the halo. This is because they typically have old stellar progenitors, with a long DWD formation time. The recently formed DWDs have a high enough frequency but have not merged yet. In a detailed study of the thin disc and

bulge contributions, Ruiter et al. (2010) show no systems with $f_{\text{GW}} > 5 \times 10^{-3}$ Hz in the bulge, claiming that the latter have all merged in by now. This is consistent with our findings, as the bulge is dominated by the He–He DWDs, which do not contribute beyond 5 mHz.

Yu & Jeffery (2010) present an axisymmetric MW model including a thin and thick disc and stellar halo with different characteristic ages for each stellar component. We confirm their distributions of the GW strain and frequency for the different binary types although they find a stronger contribution from He–He systems because of a different treatment for binary interactions. In their model, DWDs undergoing Roche lobe overflow stay in the *LISA* band and contribute at frequencies $f_{\text{GW}} > 5 \times 10^{-2}$ Hz. They conclude that most of the GW signal comes from the bulge and thin disc and that the thick disc and halo only contribute below 10^{-3} Hz. On the contrary, our Fig. 13 shows that even at high frequencies there is a significant contribution from the thick disc, and a small contribution from the halo in our simulation. We find that the DWDs detected in the halo all have $f_{\text{GW}} > 10^{-3}$ Hz, which seems necessary to generate strong signals and be detectable at larger distances. Yu & Jeffery (2010) explain that all high frequency systems in the halo and disc have merged by now, because of the age of the population. Their different result may also be related to a different binary evolution model, including a the use of the $\alpha-\gamma$ formalism for the treatment of the common envelope phase. We also note that their sample of DWDs is more than an order of magnitude smaller than ours, and undersampling may lead to the truncation of the binary distribution, especially at high frequency.

Our model is based on a cosmological simulation of a galaxy with strong resemblance to the Milky Way. However, it is not an exact reproduction of the Milky Way. In particular, its present-day star formation is about two times higher than our Milky Way (which has a low present-day star formation rate compared to other galaxies of similar mass) and the scale height of the thin and thick discs in the simulation are about twice as high as observational estimates (Sanderson et al. 2018). Although the global distribution of satellite galaxies in the simulation is comparable to the Milky Way (Wetzel et al. 2016), our simulation does not contain the equivalent of the Large Magellanic Cloud, which will likely harbour *LISA* sources. To understand the limits of our model we performed an identical analysis with the **m12f** and **m12m** simulations. In both cases we find that the total number of DWDs, as well as the number of DWDs detectable by *LISA* directly scales with the stellar mass of the Galaxy. In all simulations the signal is dominated by He–He DWDs, which are over-represented in the bulge, thick disc and stellar halo. They stem from an older, less metal-rich population. There is also a significant contribution from He–CO DWDs, which follow the stellar distribution more closely. In other words, our conclusions regarding different DWD populations are robust. However, quantitative conclusions about the detection of halo objects in the Milky Way would require a model specific model of the Milky Way satellites, which will be possible with current and future EM surveys.

Our model does not include any effects aside from binary interactions. We do not account for triple systems, which have been recently discovered, albeit with wide separations (Perpinyà-Vallès et al. 2019). We do not model DWD formation in star clusters (Kremer et al. 2018), as these low-mass binaries will likely become unbound due to dynamical interactions. We have not modelled the impact of Galactic tides on the binaries, which is negligible for very tight binaries.

The main uncertainty in our model is our choice of binary and stellar evolution parameters. We have chosen ‘standard’ assumptions (such as $\alpha = 1$ for the common envelope evolution) which are in broad agreement with the current observational constraints and enable comparison with previous work (Zorotovic et al. 2010; De Marco et al. 2011). However, the formation and evolution of the different types of white dwarfs has many uncertainties, influencing the formation time, mass distributions and separation of the binaries. Based on the same cosmological simulations, we plan a more comprehensive study of the parameter space of binary evolution to determine the range of uncertainty we currently have for *LISA* detections, both for individual systems and the unresolved background. Similarly, we leave an update of the initial binary properties for future work (Moe & Di Stefano 2017). Again, one should keep in mind that by the time *LISA* operates, many of the uncertainties will have strongly decreased thanks to EM surveys.

6 CONCLUSIONS

We have created the first double white dwarf population model based on the combination of a cosmological simulation of a Milky Way like galaxy and a binary population synthesis method. We first determine how binaries resulting from the population synthesis map on to the Milky Way galaxy and then how these binaries will be detected by *LISA*. The Milky Way model comes from a cosmological simulation, taken from the FIRE simulation suite, and provides a self-consistent model for star formation which naturally includes all the different Galactic components. Their stellar ages and distance distributions lead to distinct contributions to the gravitational wave signal by the different types of white dwarf binaries. In comparison with simplified models, our simulation produces a similar number of detectable sources but we also find many distinct features which are important for the planning of the mission and its scientific exploitation.

(i) Out of the 500 million DWDs in our simulation, over 60 million will be in the *LISA* frequency band and roughly 12 000 will be individually resolved after a nominal mission of 4 yr. The catalogue will be complete down to a frequency of a few mHz. About 15 per cent of these will be well-enough localized to allow for the search of EM counterparts with wide-field surveys.

(ii) Globally, DWDs follow a similar spatial distribution as stars and are found in all the components of the Galaxy. However, He–He systems, which have formation times up to 12 Gyr are found among older stellar populations such as the bulge, thick disc and stellar halo. Conversely CO–CO and ONe–X binaries trace young stellar populations and are found in the thin disc.

(iii) High-frequency systems ($f_{\text{GW}} > 10^{-3}$ Hz), which are the most likely to be well localized by *LISA* come from recently formed DWDs as they merge quickly, and lower frequency systems need too long time-scales to significantly reduce their period. High-frequency systems are dominated by He–He and He–CO systems, which stem from old progenitors and are strongly present in the thick disc and bulge. As such, the sky map of the well-localized systems is very different from previous realizations based on simplified models of the Galaxy.

(iv) Above 1 mHz, the Solar neighbourhood is dominated by CO–CO and He–CO binaries, while He–He binaries are five times less numerous. The high frequency systems are dominated by He–He and He–CO systems. After 2/4/8 yr of *LISA* 60/200/500 systems are expected to be well localized within 5 kpc, which is the maximal distance for detection of regular DWDs with LSST single pointings.

With stacked pointings the detection limit can reach close to 10 kpc and 3000 systems could be identified in the 8 yr catalogue.

(v) With an extended mission, we find that *LISA* would be able to detect and unambiguously locate systems beyond 50 kpc. The latter are mostly He–He binaries located in satellite galaxies and tidal streams and will have formed outside of the main galaxy.

(vi) Given our binary evolution model, 50 per cent of the resolved systems are He–CO binaries, 30 per cent are He–He binaries, 20 per cent are CO–CO binaries and there are a few per cent of binaries with a ONe WD. Over time, the fraction of He–He systems increases. As *LISA* will not be able to measure individual component masses, unambiguous classification of the sources will be limited, and model-dependent. The use of additional information may be necessary (e.g. an identified EM counterpart, or the local galactic environment) to classify the observed binaries.

(vii) Much of the most sought-after information *LISA* can provide regarding DWDs will become available after long integration times for the observations (e.g. sky localization) and will benefit from an extended mission (e.g. measurement of the chirp mass). Within the first 2 yr, less than 3 per cent of the systems will have a measured chirp mass, which increases up to 8 per cent after 4 yr and 15 per cent after 8 yr. Towards the end, *LISA* will measure the lowest chirp masses, which are likely to have the brightest EM counterparts.

These results highlight the importance of refined modelling of complete Galactic populations. It is a stepping stone for more thorough analysis of different binary population models, especially in combination with constraints from current and future EM surveys. Our new model also has implications for the preparation of *LISA* data analysis, including the unresolved gravitational wave background.

ACKNOWLEDGEMENTS

The authors would like to thank Katie Breivik, Silvia Toonen, and Valeriya Korol for many exchanges on formation channels of white dwarf binaries and Nelson Christensen and Neil Cornish for many insights on GW detections. Support for AL was provided by the Observatoire de la Côte d’Azur, the Programme National Hautes Energies with funding from the Centre National de la Recherche Scientifique (CNRS), CEA, and CNES, and NASA ATP Grant #NNX14AH35G, and NSF Collaborative Research Grant #1715847 and CAREER grant #1455342. SB is supported by the NSF Graduate Research Fellowship, grant #DGE1745303. TL acknowledges the support of NASA grant #NNH15ZDA001N and the NASA LISA Study Office. Support for SGK was provided by NSF Collaborative Research Grant #1715847 and CAREER grant #1455342, and NASA grants NNX15AT06G, JPL 1589742, and 17-ATP17-0214. This work was supported by the National Science Foundation through grant PHY 17-148958.

Some of these computations have been done on the Mesocentre SIGAMM machine, hosted by the Observatoire de la Côte d’Azur as well as cluster ‘Wheeler’ hosted by Caltech.

REFERENCES

- Abbott B. P. et al., 2017, *Phys. Rev. Lett.*, 119, 161101
 Abt H. A., 1983, *ARA&A*, 21, 343
 Amaro-Seoane P. et al., 2017, preprint ([arXiv:1702.00786](https://arxiv.org/abs/1702.00786))
 Bellm E. C. et al., 2019, *PASP*, 131, 018002
 Bonaca A., Conroy C., Wetzel A., Hopkins P. F., Kereš D., 2017, *ApJ*, 845, 101
 Breivik K., Kremer K., Bueno M., Larson S. L., Coughlin S., Kalogera V., 2018, *ApJ*, 854, L1
 Brown W. R., Kilic M., Allende Prieto C., Kenyon S. J., 2010a, *ApJ*, 723, 1072
 Brown W. R., Kilic M., Allende Prieto C., Kenyon S. J., 2010b, *ApJ*, 723, 1072
 Brown W. R., Gianninas A., Kilic M., Kenyon S. J., Allende Prieto C., 2016a, VizieR Online Data Catalog, p. J/ApJ/818/155
 Brown W. R., Gianninas A., Kilic M., Kenyon S. J., Allende Prieto C., 2016b, *ApJ*, 818, 155
 Brown W. R., Kilic M., Kenyon S. J., Gianninas A., 2016c, *ApJ*, 824, 46
 Claeys J. S. W., Pols O. R., Izzard R. G., Vink J., Verbunt F. W. M., 2014, *A&A*, 563, A83
 Cooray A., Seto N., 2005, *ApJ*, 623, L113
 Cornish N. J., Littenberg T. B., 2007, *Phys. Rev. D*, 76, 083006
 Cornish N., Robson T., 2017, *J. Phys. Conf. Ser.*, 840, 012024
 Crowder J., Cornish N. J., 2007, *Phys. Rev. D*, 75, 043008
 Cutler C., Flanagan E. E., 1994, *Phys. Rev. D*, 49, 2658
 De Marco O., Passy J.-C., Moe M., Herwig F., Mac Low M.-M., Paxton B., 2011, *MNRAS*, 411, 2277
 Escala I. et al., 2018, *MNRAS*, 474, 2194
 Garrison-Kimmel S. et al., 2017, *MNRAS*, 471, 1709
 Gokhale V., Peng X. M., Frank J., 2007, *ApJ*, 655, 1010
 Graham M. J. et al., 2019, *PASP*, 131, 078001
 Heggie D. C., 1975, *MNRAS*, 173, 729
 Hopkins P. F., 2015, *MNRAS*, 450, 53
 Hopkins P. F., Kereš D., Oñorbe J., Faucher-Giguère C.-A., Quataert E., Murray N., Bullock J. S., 2014, *MNRAS*, 445, 581
 Hopkins P. F. et al., 2018, *MNRAS*, 480, 800
 Hurley J. R., Tout C. A., Pols O. R., 2002a, *MNRAS*, 329, 897
 Hurley J. R., Tout C. A., Pols O. R., 2002b, *MNRAS*, 329, 897
 Iben I. J., Tutukov A. V., 1984, *ApJS*, 54, 335
 Ivanova N. et al., 2013, *A&AR*, 21, 59
 Ivezić Ž. et al., 2019, *ApJ*, 873, 111
 Iwamoto K., Brachwitz F., Nomoto K., Kishimoto N., Umeda H., Hix W. R., Thielemann F.-K., 1999, *ApJS*, 125, 439
 Izzard R. G., Tout C. A., Karakas A. I., Pols O. R., 2004, *MNRAS*, 350, 407
 Korol V., Rossi E. M., Groot P. J., Nelemans G., Toonen S., Brown A. G. A., 2017, *MNRAS*, 470, 1894
 Korol V., Koop O., Rossi E. M., 2018, *ApJ*, 866, L20
 Korol V., Rossi E. M., Barausse E., 2019, *MNRAS*, 483, 5518
 Kremer K., Breivik K., Larson S. L., Kalogera V., 2017, *ApJ*, 846, 95
 Kremer K., Chatterjee S., Breivik K., Rodriguez C. L., Larson S. L., Rasio F. A., 2018, *Phys. Rev. Lett.*, 120, 191103
 Kroupa P., 2001, *MNRAS*, 322, 231
 Kupfer T. et al., 2018, *MNRAS*, 480, 302
 Lamberts A. et al., 2018, *MNRAS*, 480, 2704
 Levitan D. et al., 2013, *MNRAS*, 430, 996
 Littenberg T. B., 2011, *Phys. Rev. D*, 84, 063009
 Ma X., Hopkins P. F., Wetzel A. R., Kirby E. N., Anglés-Alcázar D., Faucher-Giguère C.-A., Kereš D., Quataert E., 2017, *MNRAS*, 467, 2430
 Marigo P., 2001, *A&A*, 370, 194
 Marsh T. R., 2011, *Class. Quantum Gravity*, 28, 094019
 Marsh T. R., Nelemans G., Steeghs D., 2004, *MNRAS*, 350, 113
 Moe M., Di Stefano R., 2017, *ApJS*, 230, 15
 Napiwotzki R. et al., 2001, *Astron. Nachr.*, 322, 411
 Nelemans G., Portegies Zwart S. F., Verbunt F., Yungelson L. R., 2001a, *A&A*, 368, 939
 Nelemans G., Yungelson L. R., Portegies Zwart S. F., 2001b, *A&A*, 375, 890
 Nisanke S., Vallisneri M., Nelemans G., Prince T. A., 2012, *ApJ*, 758, 131
 Nomoto K., Tominaga N., Umeda H., Kobayashi C., Maeda K., 2006, *Nucl. Phys. A*, 777, 424
 Perpinya-Vallès M., Rebassa-Mansergas A., Gänsicke B. T., Toonen S., Hermes J. J., Gentile Fusillo N. P., Tremblay P. E., 2019, *MNRAS*, 483, 901
 Peters P. C., Mathews J., 1963, *Phys. Rev.*, 131, 435

- Planck Collaboration XIII, 2016, *A&A*, 594, A13
 Postnov K. A., Yungelson L. R., 2014, *Living Rev. Relativ.*, 17, 3
 Prantzos N., Boissier S., 2000, *MNRAS*, 313, 338
 Rebassa-Mansergas A. et al., 2012, *MNRAS*, 423, 320
 Ruiter A. J., Belczynski K., Benacquista M., Holley-Bockelmann K., 2009, *ApJ*, 693, 383
 Ruiter A. J., Belczynski K., Benacquista M., Larson S. L., Williams G., 2010, *ApJ*, 717, 1006
 Saio H., Nomoto K., 2004, *ApJ*, 615, 444
 Sanderson R. E. et al., 2018, preprint ([arXiv:1806.10564](https://arxiv.org/abs/1806.10564))
 Sharma S., Johnston K. V., 2009, *ApJ*, 703, 1061
 Shen K. J., 2015, *ApJ*, 805, L6
 Shen K. J., Bildsten L., Kasen D., Quataert E., 2012, *ApJ*, 748, 35
 Strader J. et al., 2018, preprint ([arXiv:1811.12433](https://arxiv.org/abs/1811.12433))
 Street R. A. et al., 2018, preprint ([arXiv:1812.03137](https://arxiv.org/abs/1812.03137))
 Su K.-Y., Hopkins P. F., Hayward C. C., Faucher-Giguère C.-A., Kereš D., Ma X., Robles V. H., 2017, *MNRAS*, 471, 144
 The LIGO Scientific Collaboration, 2019, GWTC-1: A gravitational wave transient catalog of compact binaries observed by LIGO and Virgo during the first and second observing runs, *Phys. Rev. X*, 9, 031040
 Timpano S. E., Rubbo L. J., Cornish N. J., 2006, *Phys. Rev. D*, 73, 122001
 Toonen S., Nelemans G., Portegies Zwart S., 2012, *A&A*, 546, A70
 Toonen S., Voss R., Knigge C., 2014a, *MNRAS*, 441, 354
 Toonen S., Claeys J. S. W., Mennekens N., Ruiter A. J., 2014b, *A&A*, 562, A14
 Toonen S., Hollands M., Gänsicke B. T., Boekholt T., 2017, *A&A*, 602, A16
 Tout C. A., Aarseth S. J., Pols O. R., Eggleton P. P., 1997, *MNRAS*, 291, 732
 Vallisneri M., 2008, *Phys. Rev. D*, 77, 042001
 van den Hoek L. B., Groenewegen M. A. T., 1997, *A&AS*, 123, 305
 Vink J. S., de Koter A., Lamers H. J. G. L. M., 2001, *A&A*, 369, 574
 Wetzel A. R., Hopkins P. F., Kim J.-H., Faucher-Giguère C.-A., Kereš D., Quataert E., 2016, *ApJ*, 827, L23
 Yu S., Jeffery C. S., 2010, *A&A*, 521, A85
 Yu S., Jeffery C. S., 2013, *MNRAS*, 429, 1602
 Zorotovic M., Schreiber M. R., Gänsicke B. T., Nebot Gómez-Morán A., 2010, *A&A*, 520, A86

This paper has been typeset from a TeX/LaTeX file prepared by the author.